SCIENTIFIC REPORTS

OPEN

Intracellular Chloride Regulation in AVP+ and VIP+ Neurons of the Suprachiasmatic Nucleus

Received: 23 March 2017
Accepted: 28 July 2017
Published online: 31 August 2017

Nathan J. Klett[1,2] & Charles N. Allen[2,3]

Several reports have described excitatory GABA transmission in the suprachiasmatic nucleus (SCN), the master pacemaker of circadian physiology. However, there is disagreement regarding the prevalence, timing, and neuronal location of excitatory GABA transmission in the SCN. Whether GABA is inhibitory or excitatory depends, in part, on the intracellular concentration of chloride ($[Cl^-]_i$). Here, using ratiometric Cl^- imaging, we have investigated intracellular chloride regulation in AVP and VIP-expressing SCN neurons and found evidence suggesting that $[Cl^-]_i$ is higher during the day than during the night in both AVP+ and VIP+ neurons. We then investigated the contribution of the cation chloride cotransporters to setting $[Cl^-]_i$ in these SCN neurons and found that the chloride uptake transporter NKCC1 contributes to $[Cl^-]_i$ regulation in SCN neurons, but that the KCCs are the primary regulators of $[Cl^-]_i$ in SCN neurons. Interestingly, we observed that $[Cl^-]_i$ is differentially regulated between AVP+ and VIP+ neurons-a low concentration of the loop diuretic bumetanide had differential effects on AVP+ and VIP+ neurons, while blocking the KCCs with VU0240551 had a larger effect on VIP+ neurons compared to AVP+ neurons.

The suprachiasmatic nucleus (SCN) of the anterior hypothalamus is the master pacemaker of the circadian system. Besides a cohort of neuropeptides, SCN neurons synthesize and package the neurotransmitter GABA. GABA transmission regulates synaptic input from the RHT[1], mediates phase shifts[2,3], regulates firing frequency[4], and contributes to circadian synchrony[5–9].

GABA is the primary inhibitory neurotransmitter in the central nervous system, but has been observed to be excitatory during embryonic and neonatal development, in certain pathologies, as well as in several areas of the adult brain[10–12]. Interestingly, excitatory GABA transmission has been observed in the mature SCN[6,7,13–20]. However, reports have disagreed on the prevalence, timing, and neuronal location of excitatory GABA transmission. GABA has been reported to be exclusively inhibitory, inhibitory during the day and excitatory during the night, and excitatory during the night and inhibitory during the day[7,13–15,17,20–22]. Additionally, the proportion of neurons within the SCN neural network that are excited by GABA may be involved in encoding day length[18,23].

The $GABA_A$ receptor is permeable to both Cl^- and HCO_3^- ions with a relative permeability ratio of approximately 0.8[24–26]. Because the $GABA_A$ receptor is primarily permeable to Cl^- ions, whether GABA is depolarizing or hyperpolarizing depends on the intracellular concentration of chloride ($[Cl^-]_i$) and the membrane potential. $[Cl^-]_i$ is regulated by a family of cation chloride cotransporters (CCCs) which use the concentration gradients of Na^+ and K^+ ions to transport Cl^- ions into (the sodium-potassium-chloride cotransporter 1, NKCC1) or out of (the potassium-chloride cotransporters, KCC) neurons. Normally, $[Cl^-]_i$ is kept low in neurons by the action of the neuron-specific[27,28] isotonically-active[29–31] KCC2. However, a role for NKCC1 in $[Cl^-]_i$ regulation has been demonstrated in the SCN—blocking NKCC1 with bumetanide decreased the amplitude of GABA-induced Ca^{2+} transients[15,16,18] and hyperpolarized the GABAergic reversal potential[15,17].

Interestingly, immunohistochemistry has revealed differential expression of chloride transporters throughout the SCN[32]. KCC2 expression was most dense in the ventrolateral SCN, and correlated with vasoactive intestinal peptide (VIP) expression. Alternatively, KCC3 and KCC4 expression was concentrated in the dorsomedial SCN. NKCC1 was expressed throughout the SCN, but was concentrated in the dorsomedial SCN, and correlated with

[1]Neuroscience Graduate Program, School of Medicine, Oregon Health & Science University, Portland, OR, 97239, USA. [2]Oregon Institute for Occupational Health Sciences, School of Medicine, Oregon Health & Science University, Portland, OR, 97239, USA. [3]Department of Behavioral Neuroscience, School of Medicine, Oregon Health & Science University, Portland, OR, 97239, USA. Correspondence and requests for materials should be addressed to C.N.A. (email: allenc@ohsu.edu)

vasopressin (AVP) expression. The differential expression of the CCCs throughout the SCN suggests that $[Cl^-]_i$ and the GABAergic equilibrium potential (E_{GABA}) may vary regionally throughout the SCN. Indeed, Albus *et al*. observed that GABA is exclusively inhibitory in the ventral SCN, but is excitatory in the dorsal SCN during the late day and early night[6]. Similarly, GABA-induced Ca^{2+} transients were found to be most prevalent in the dorsomedial SCN[16], and using the Cl^--sensitive dye MQAE, $[Cl^-]_i$ was found to be elevated in the dorsomedial SCN[9]. Therefore, there is mounting evidence to support the idea that subpopulations of SCN neurons differ in their regulation of the intracellular chloride concentration.

In this work, we used epifluorescent imaging of a genetically-encoded chloride indicator to examine regional and circadian regulation of $[Cl^-]_i$ in the SCN. Cl-Sensor is a ratiometric chloride indicator composed of a CFP moiety linked to a YFP moiety whose emission is sensitive to chloride in a physiological range (YFP_{Cl}). Ratiometric Cl^- imaging allows estimation of $[Cl^-]_i$ from multiple cells simultaneously without disrupting the native cellular milieu. Using a transgenic strategy, we targeted Cl-Sensor to AVP or VIP-expressing SCN neurons, and were able to detect both transient and persistent changes in $[Cl^-]_i$.

Our results indicate that $GABA_A$ receptor activation elicits Cl^- influx in AVP+ and VIP+ neurons in the SCN. Accordingly, we show that the KCCs play a major role in $[Cl^-]_i$ regulation in SCN neurons, while the chloride importer NKCC1 has a relatively minor role in setting resting $[Cl^-]_i$. Further, we show that $[Cl^-]_i$ is differentially regulated in AVP and VIP-expressing neurons.

Results

Vasoactive intestinal peptide (VIP) and vasopressin (AVP) mark the "core" and "shell" partition that has served as a useful anatomical model for dissecting SCN function. Generally, sensory inputs project to the ventrolateral SCN core, while core neurons synapse unto neurons in the dorsomedial shell. Several reports have suggested that excitatory GABA transmission may correlate with this anatomical feature[13–15,17,20]. Therefore, we performed Cl^- imaging in VIP+ and AVP+ neurons of the SCN to look for differences in $[Cl^-]_i$ regulation between these two populations of neurons. To measure $[Cl^-]_i$ in SCN neurons, we used a newly-developed Cre-inducible mouse line, with a floxed Cl-Sensor allele inserted into the Rosa26 locus[33]. To obtain Cl-Sensor expression in the SCN, we crossed these mice with either VIP-IRES-Cre mice or AVP-IRES-Cre mice to give Cl-Sensor expression in either VIP+ or AVP+ neurons[34,35]. The resultant VIP::Cl-Sensor mice displayed Cl-Sensor expression in the ventrolateral SCN, while the AVP::Cl-Sensor mice displayed Cl-Sensor expression in the dorsomedial SCN, as expected for VIP and AVP expression (Fig. 1A,B[36]).

Several studies have indicated that excitatory GABA transmission demonstrates circadian rhythmicity[13,14,16,17,20]. Therefore, we first compared baseline values of R_{Cl} during the day (ZT 2 to 8) and night (ZT 12 to 18) in AVP+ and VIP+ SCN neurons. Interestingly, R_{Cl} was higher during the day in both AVP+ (generalized estimating equations (GEE), $p < 0.05$) and VIP+ (GEE, $p < 0.001$) neurons (Fig. 1E) suggesting that $[Cl^-]_i$ is higher during the day in these neurons. Several reports have described regional variability of excitatory GABA transmission, with some agreement that it is more common in the dorsal SCN, suggesting that this phenomenon may be specific to AVP+ neurons. Indeed, in the nearby paraventricular nucleus, Haam *et al*. observed that AVP+ neurons had a more depolarized E_{GABA} relative to their AVP− neighbors[37]. To determine whether AVP+ neurons demonstrate higher $[Cl^-]_i$ relative to VIP+ neurons, we compared baseline R_{Cl} values between VIP+ and AVP+ neurons, but found no significant difference in R_{Cl} during either the day or the night (Fig. 1E).

A hyperpolarizing action of GABA will elicit Cl^- influx, while a depolarizing action will elicit Cl^- efflux. To assess the polarity of GABA transmission in SCN neurons, we performed puff applications of the $GABA_A$ agonist isoguvacine in the presence of 2 µM TTX to block potential polysynaptic effects. In response, R_{Cl} increased in AVP+ neurons during the day and night, indicative of Cl^- influx and inhibitory GABA transmission (Fig. 2, top row). Cl^- influx was also observed in VIP+ neurons during both the day and the night (Fig. 2, bottom row). These results indicate that GABA is inhibitory in both AVP+ and VIP+ SCN neurons. Interestingly, these $GABA_A$-induced Cl^- transients lasted for minutes, much longer than expected for $GABA_A$-induced currents, but similar to the timecourse of Cl^- transients reported in other cells[38–40]. The timecourse of these Cl^- transients may represent the activity of chloride transporters. Indeed, it has been shown that transient shifts in GABA polarity can last for minutes and that chloride transporters mediate this equilibration process[41–43].

Therefore, we next examined the degree to which the CCCs set $[Cl^-]_i$ in SCN neurons. Since our $GABA_A$-induced Cl^- transients indicated inhibitory Cl^- influx upon $GABA_A$ receptor activation, we first investigated the contribution of KCC2, the neuron-specific CCC responsible for keeping $[Cl^-]_i$ levels low in neurons throughout the brain. To test for the activity of KCC2 in setting resting $[Cl^-]_i$ we used VU0240551, an antagonist that selectively targets the KCCs[44]. VU increased R_{Cl} by 0.18 in AVP+ and by 0.27 in VIP+ neurons (Fig. 3A,B). Based on our calibration curve (Supplementary Fig. 1), we estimate these changes in R_{Cl} to reflect a 15 mM increase in $[Cl^-]_i$ in AVP+ neurons and a 29 mM increase in VIP+ neurons. VU had a significantly greater effect in VIP+ neurons compared to AVP+ neurons (GEE, $p < 0.05$), but there were no day/night differences within neuron type (Fig. 3C). Because several Cl^- transporters are also transporters for the bicarbonate ion, we wondered if removing bicarbonate ions from the extracellular solution might alter $[Cl^-]_i$ and therefore the efficacy of VU. Therefore, we repeated VU application in a separate set of experiments using a HEPES-buffered solution (Fig. 3D). Blocking the KCCs with VU gave a pattern of results similar to that observed with solution containing bicarbonate. VU elicited an increase in R_{Cl} in all conditions, indicative of $[Cl^-]_i$ increase. When comparing the effect of VU across solutions, we observed a difference in the amplitude of VU's effect in AVP+ neurons during the day (two-sample *z*-test, $p < 0.05$). Furthermore, experiments in HEPES solution revealed a day/night difference in the effect of VU that was not present in the bicarbonate solution (Fig. 3D, GEE, $p < 0.05$). In a separate set of experiments, we examined the effect of VU on the GABAergic reversal potential (E_{GABA}) using perforated-patch recording. In these experiments, VU elicited a depolarization of E_{GABA} by approximately 23 mV (paired *t*-test, $p < 0.001$), and slowed the recovery of resting E_{GABA} after Cl^- loading (paired *t*-test, $p < 0.05$)

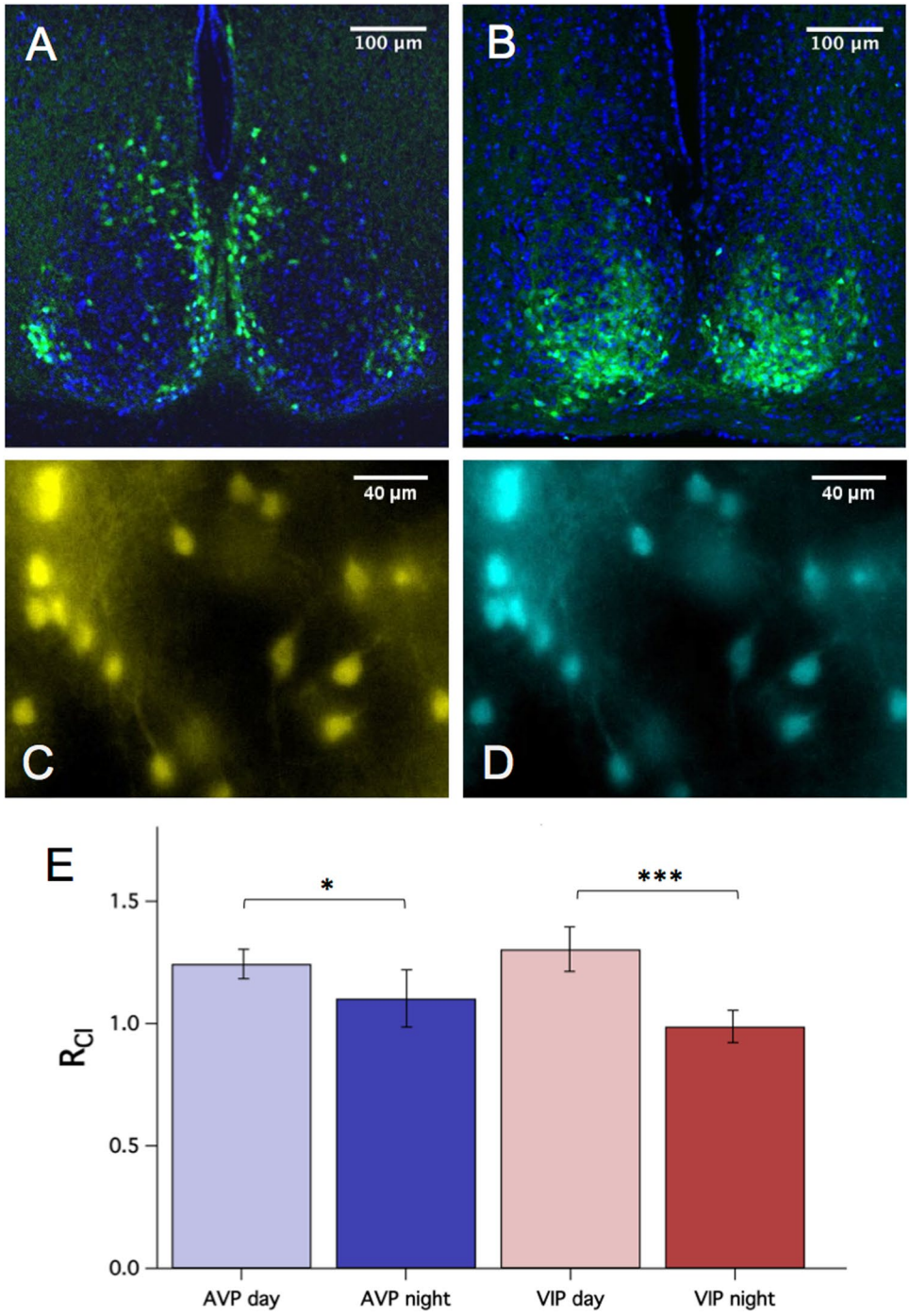

Figure 1. R_{Cl} measurement in genetically-identified SCN neurons. Confocal micrographs demonstrating regional expression of Cl-Sensor in the SCN of AVP::Cl-Sensor (**A**) and VIP::Cl-Sensor (**B**) mice. Native Cl-Sensor fluorescence is depicted in green, and DAPI stain is shown in blue. Pseudocolored epifluorescent micrographs of an AVP::Cl-Sensor SCN slice exhibiting YFP (**C**) and CFP (**D**) emission. (**E**) Baseline R_{Cl} was higher during the day (ZT 2 to 8) compared to the night (ZT 12 to 18) for both AVP+ (GEE, $p < 0.05$) and VIP+ (GEE, $p < 0.001$) neurons.

(see Supplementary Fig. 2). Collectively, we interpret these findings to indicate that the KCC family of chloride cotransporters play a major role in $[Cl^-]_i$ regulation in SCN neurons.

Previous studies have implicated NKCC1 in $[Cl^-]_i$ regulation in SCN neurons[15–18,32]. To test for a contribution of NKCC1 to resting $[Cl^-]_i$, we used the loop diuretic bumetanide which selectively targets NKCC1 when used at 10 µM[45]. Bumetanide increased R_{Cl} in AVP+ neurons by approximately 0.04 (~4 mM) and decreased R_{Cl} in VIP+ neurons by 0.04 (~3 mM) (Fig. 4). These changes were small but significantly different from baseline (GEE, $p < 0.005$). As with VU, we observed differences in the effect of bumetanide between AVP+ and VIP+

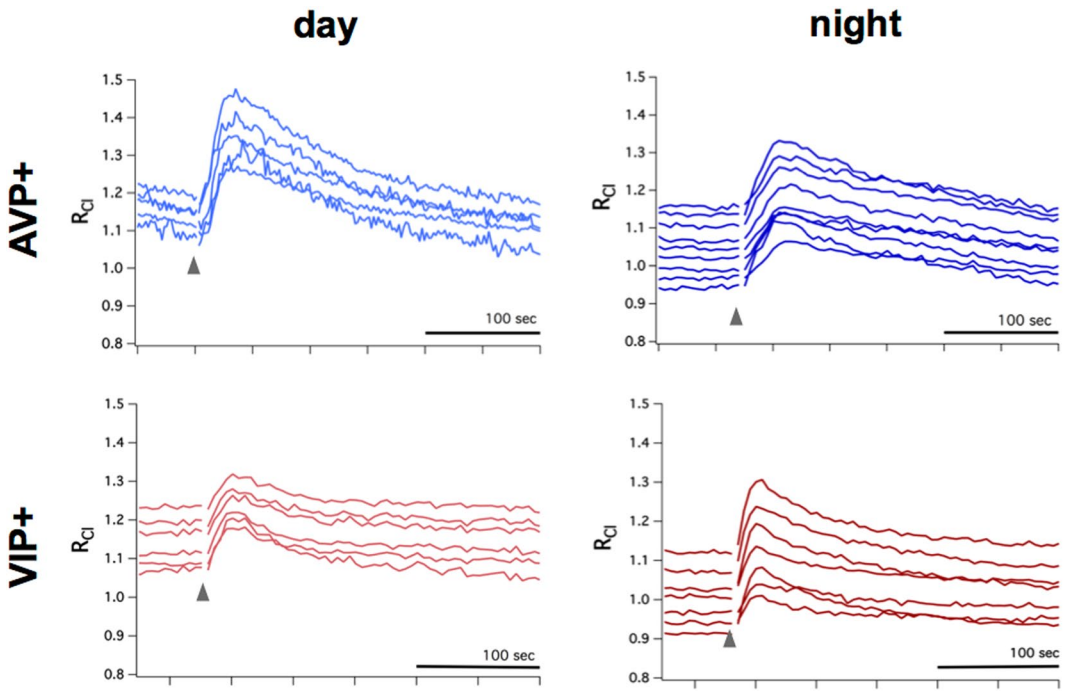

Figure 2. $GABA_A$ receptor-mediated Cl^- transients in AVP+ and VIP+ neurons. Top row: AVP+ neurons from AVP::Cl-Sensor mice tested during subjective day (left) and subjective night (right) demonstrated an increase of R_{Cl} following puff application of the $GABA_A$ agonist isoguvacine (gray arrow), indicative of inhibitory Cl^- influx. Similarly, VIP+ neurons from VIP::Cl-Sensor mice during both day and night responded to isoguvacine with an increase of R_{Cl} (bottom row). Each trace represents a R_{Cl} measurement obtained from a single neuronal soma.

neurons (GEE, $p < 0.001$), but no day/night differences within neuron type. Surprisingly, bumetanide elicited a small increase in $[Cl^-]_i$ in AVP+ neurons, contrary to its expected role in blocking Cl^- uptake. This result may be due to off-target effects of bumetanide, which is known to inhibit the KCCs at higher concentrations[10,44]. In a separate series of experiments, we tested the efficacy of bumetanide in a HEPES-buffered solution, which should diminish Cl^-/HCO_3^- exchange. In HEPES, bumetanide reduced R_{Cl} in VIP+ neurons but had little effect on AVP+ neurons (Fig. 4D). However, the effect of bumetanide on AVP+ neurons was significantly greater in the bicarbonate-buffered solution compared to the HEPES-buffered solution (two-sample z-test, $p < 0.05$). As in the bicarbonate-buffered experiments, bumetanide elicited a greater effect in VIP+ neurons compared to AVP+ neurons (GEE, $p < 0.05$). Using perforated-patch recording, we also investigated the effect of bumetanide on E_{GABA}. In these experiments, bumetanide did not significantly alter E_{GABA} or the timecourse for the recovery of E_{GABA} following a Cl^- depletion protocol (Supplementary Fig. 3). Overall, we observed relatively small effects of bumetanide compared to VU, suggesting that the KCCs are the major regulators of resting $[Cl^-]_i$ in SCN neurons.

The previous results indicate that both NKCC1 and the KCC family of cotransporters contribute to resting $[Cl^-]_i$ in SCN neurons. We next investigated how these cotransporters interact to regulate $[Cl^-]_i$. As discussed, blocking the KCCs with VU resulted in a substantial increase in R_{Cl} (Fig. 3). However, because of the relatively minor effect of bumetanide, it was not clear what Cl^- uptake pathways were mediating the effect of VU. In order to determine if NKCC1 mediates Cl^- uptake in the absence of the KCCs, we applied VU after bumetanide treatment (Fig. 5A). The effect of VU was largely occluded in the presence of bumetanide (Fig. 5A,B). Therefore, although NKCC1 has a relatively minor role in setting resting $[Cl^-]_i$, it does constitute a tonic Cl^- influx pathway in SCN neurons. Conversely, we next examined whether blocking the KCCs could reveal a greater bumetanide effect. However, the amplitude of bumetanide's effect was similar in the presence or absence of VU (Fig. 5C,D), indicating that the KCCs are necessary for Cl^- extrusion.

Discussion

We performed somatic Cl^- imaging to investigate $[Cl^-]_i$ in two genetically-defined subpopulations of SCN neurons. We found that R_{Cl} was higher in both AVP+ and VIP+ neurons during the day (ZT 2 to 8) compared to the night (ZT 12 to 18), suggesting that $[Cl^-]_i$ is elevated during the day. This observation is in agreement with several reports that have observed increased excitatory GABA transmission during the day and early night[6,13,15–17]. However, we observed Cl^- influx in response to $GABA_A$ receptor activation, indicative of an inhibitory effect of GABA. Similarly, we observed large changes in R_{Cl} after application of the KCC antagonist VU, but small changes after blocking NKCC1 with bumetanide. VU increased $[Cl^-]_i$ dramatically, in the range of 15 to 30 mM, suggesting that the KCCs are the major determinants of $[Cl^-]_i$ in AVP+ and VIP+ SCN neurons. Therefore, our results add to a group of studies that have concluded that GABA is exclusively inhibitory in the mature SCN[5,46–49]. Still,

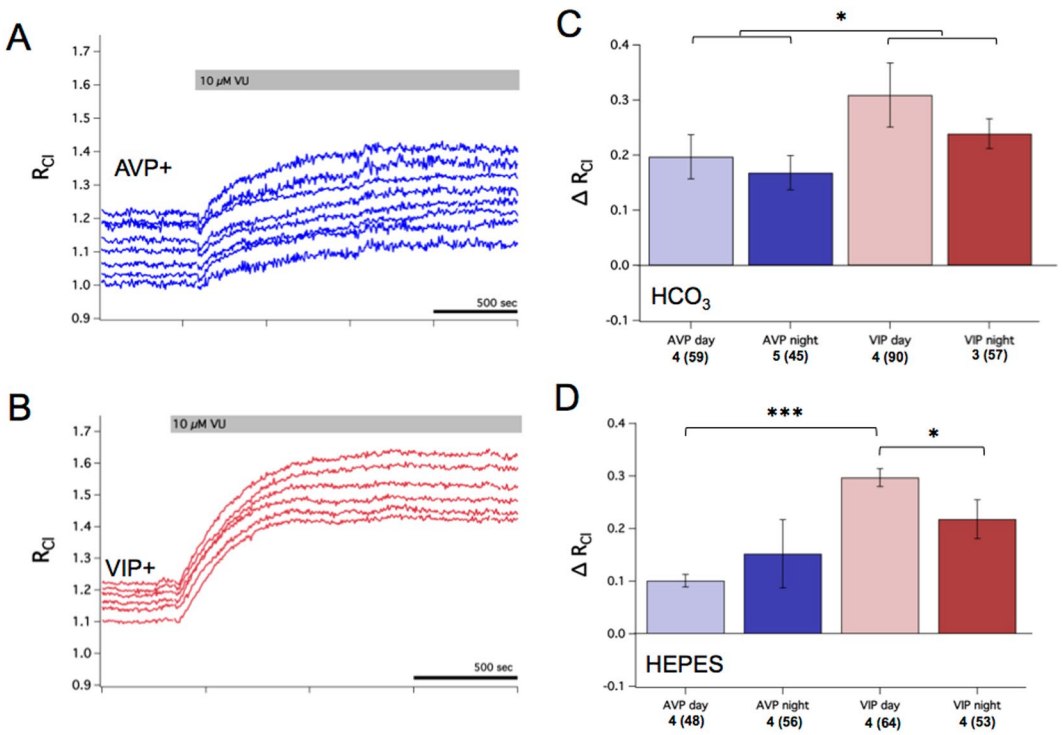

Figure 3. The KCCs regulate $[Cl^-]_i$ in SCN neurons. (**A**) Example experiment from an AVP::Cl-Sensor mouse recorded during the night demonstrating the effect of 10 μM of the KCC antagonist VU. VU caused an increase in R_{Cl} indicative of a rise in $[Cl^-]_i$. Each trace represents a R_{Cl} measurement obtained from a single neuronal soma. (**B**) Example experiment from a VIP::Cl-Sensor mouse recorded during the day demonstrating the effect of VU. VU caused an increase in R_{Cl} indicative of a rise in $[Cl^-]_i$. (**C**) Summary data of the average change in R_{Cl} after VU by neuron type and time of day. VU resulted in an increase in R_{Cl} in all conditions (GEE, $p < 0.005$), but had a significantly greater effect in VIP+ neurons compared to AVP+ neurons (GEE, $p < 0.05$). (**D**) Summary of changes in R_{Cl} elicited by VU in a HEPES-buffered solution. VU had a larger effect during the day in VIP+ neurons when compared to VIP+ night (GEE, $p < 0.05$) and AVP+ day neurons (GEE, $p < 0.001$). For (**C**) and (**D**), the number of slices and total regions of interest (in parentheses) is listed for each condition under the x-axis.

it should be remembered that the SCN is a very heterogeneous nuclei and that AVP and VIP-expressing neurons only constitute ~13% and ~9% of all SCN neurons respectively[50,51], leaving open the possibility that our study did not address the SCN neurons demonstrating excitatory GABA.

The descriptions of excitatory GABA transmission in the SCN have been riddled with discrepancies. Differences in methodology are likely to underlie some of these inconsistencies. Indeed, whole-cell, perforated-patch, cell-attached, and multi-unit recording techniques as well as Ca^{2+} imaging have all been used to address the polarity of GABA transmission in the SCN. The timing of inhibitory post-synaptic currents within the interspike interval is critical in determining whether inhibitory currents will speed up or slow cell firing, further highlighting the nuance of GABA transmission in the SCN[4,9,52]. The issue may also be related to the complexity of intracellular Cl^- regulation itself. Besides neurotransmission, $[Cl^-]_i$ is an important cellular feature linked to processes such as pH regulation, cell volume regulation, and even membrane potential[12,43,54]. Therefore, cell turgidity as well as the osmolarity and pH of solutions are all likely to influence measures of $[Cl^-]_i$. Further, $[Cl^-]_i$ has been shown to change after neuronal damage, and in relation to the proximity of cells to the surface of a brain slice[55,56]. Additionally, previous studies have not adequately ruled out the possibility that disinhibition underlies the observed excitatory effects of GABA transmission in the SCN. The SCN network is known to have diffuse local connectivity[7,19,57]. Therefore, polysynaptic effects must be considered when applying GABA agonists to SCN neurons. Without the inclusion of TTX in the recording media, GABA-mediated inhibition of pre-synaptic inputs could be read out as excitation in the cell of interest. Further, some of the data in support of excitatory GABA transmission has been inferred by the effects of the $GABA_A$ receptor antagonist bicuculline[14,15,58]. Regrettably, these results are confounded by the off-target effects of bicuculline, which is known to antagonize SK channels at commonly used concentrations[59]. Indeed, SK channels have been shown to contribute to the resting membrane potential, afterhyperpolarization and spike-frequency adaptation of SCN neurons[60,61].

We have successfully performed Cl^- imaging techniques in SCN neurons, and have demonstrated their utility for monitoring Cl^- flux and $[Cl^-]_i$ regulation. Cl^- imaging offers several advantages compared to gramicidin perforated patch recording by leaving V_m unperturbed and by allowing for the sampling of multiple neurons

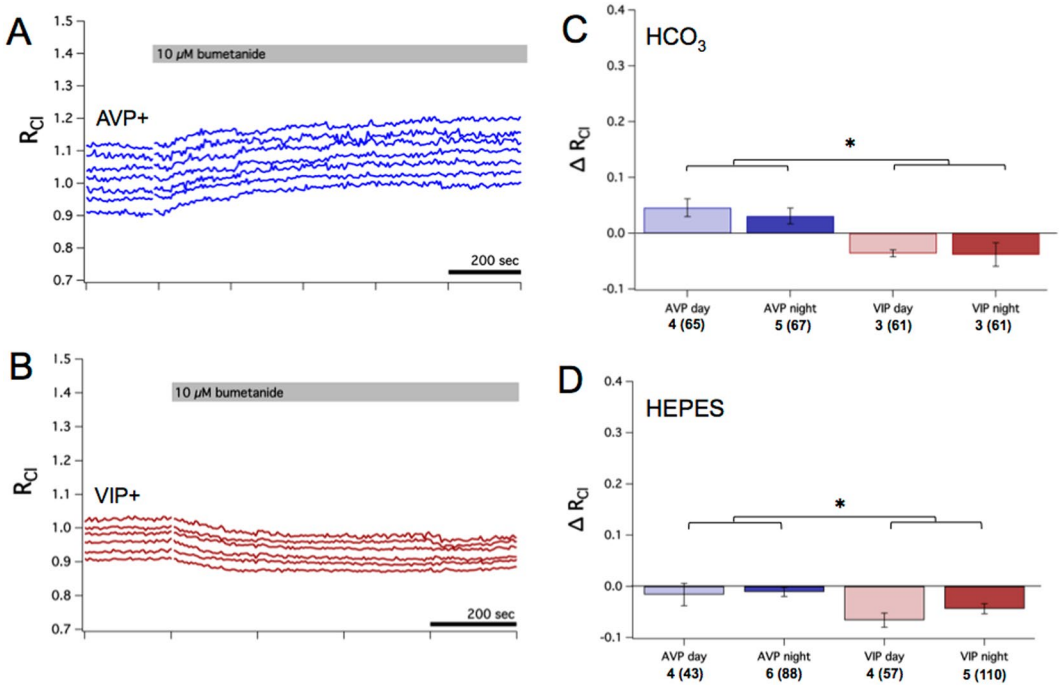

Figure 4. NKCC1 contributes to setting resting $[Cl^-]_i$ in SCN neurons. (**A**) Example experiment from an AVP::Cl-Sensor mouse recorded during the night showing the effect of blocking NKCC1 with 10 μM of bumetanide. Bumetanide caused a small increase in R_{Cl}. Each trace represents a R_{Cl} measurement obtained from a single neuronal soma. (**B**) Example experiment from a VIP::Cl-Sensor mouse recorded during the night demonstrating the effect of bumetanide. Bumetanide caused a small decrease in R_{Cl}. (**C**) Summary data of the average change in R_{Cl} after bumetanide by neuron type and time of day. Bumetanide elicited small but statistically significant changes in R_{Cl} in each condition (GEE, $p < 0.005$). AVP+ and VIP+ neurons responded differently to bumetanide (GEE, $p < 0.001$), but there were no day/night differences within neuron types. Bumetanide had a statistically different effect on VIP+ neurons compared to AVP+ neurons. (**D**) Summary of changes in R_{Cl} elicited by bumetanide in a HEPES-buffered solution. Bumetanide had a larger effect in AVP+ neurons compared to VIP+ neurons (GEE, $p < 0.001$). For (**C**) and (**D**), the number of slices and total regions of interest (in parentheses) is listed for each condition under the x-axis.

simultaneously. Further, the use of a genetically-encoded indicator allowed us to target specific populations of SCN neurons. Nevertheless, Cl-Sensor has room for improvement. Cl-Sensor's sensitivity to Cl^- is not optimal for normal neuronal concentrations of chloride, and the intrinsic H^+ sensitivity of the indicator within a physiological pH range can be problematic.

Our methodology did not allow us to investigate subcellular differences in R_{Cl}. Indeed, intracellular Cl^- gradients have been reported in several types of neurons throughout the brain (see[62] for review). For example, a two-photon Cl^- imaging study observed a somatodendritic chloride gradient in a class of retinal bipolar cells, concluding that Cl^- is 20 mM higher in dendrites relative to the soma[63]. A somatodendritic Cl^- gradient could explain why previous studies have shown GABA-evoked Ca^{2+} transients in SCN neurons[15,16,18], supporting an excitatory role of GABA, while we have observed inhibitory Cl^- influx. While dendritic depolarization may be able to activate somatic voltage-gated calcium channels, Cl^- efflux at dendrites may not be registered by somatic Cl^- imaging. Similarly, a somatodendritic Cl^- gradient could explain why bumetanide was able to diminish GABA-evoked Ca^{2+} transients, but produced small changes in our measurements of somatic R_{Cl}. Higher-resolution imaging techniques will be necessary to address whether somatodendritic Cl^- gradients exist in SCN neurons.

Recently, the role of the CCC's in determining $[Cl^-]_i$ has come under scrutiny by compelling two-photon Cl^- imaging results which argue for the primacy of large intracellular anions in setting $[Cl^-]_i$[64]. In their study, Glycks *et al.* observed little effect of blocking either NKCC1 or KCC2 in hippocampal and neocortical pyramidal neurons, while we found a small effect of bumetanide and a clear effect of VU. Neuron type could underlie this incongruity. Alternatively, while we monitored R_{Cl} continuously, Glycks *et al.* sampled R_{Cl} before and 30 minutes after application of bumetanide and VU, leaving open the possibility that secondary homeostatic mechanisms reset $[Cl^-]_i$ during that time.

Although we did not observe a difference in resting R_{Cl} between AVP+ and VIP+ neurons, we did observe differential regulation of $[Cl^-]_i$ between AVP+ and VIP+ neurons. We found that AVP+ and VIP+ neurons differed in their sensitivity to both VU and bumetanide. The increased sensitivity of VIP+ neurons to VU suggests that they may have lower resting $[Cl^-]_i$ relative to AVP+ neurons, consistent with studies that have observed a greater prevalence of excitatory GABA transmission in the dorsal SCN[6,15,16] as well as with recent data from two groups who, using the Cl^- sensitive dye MQAE, concluded that $[Cl^-]_i$ is elevated in the dorsal SCN[9,23]. Previous

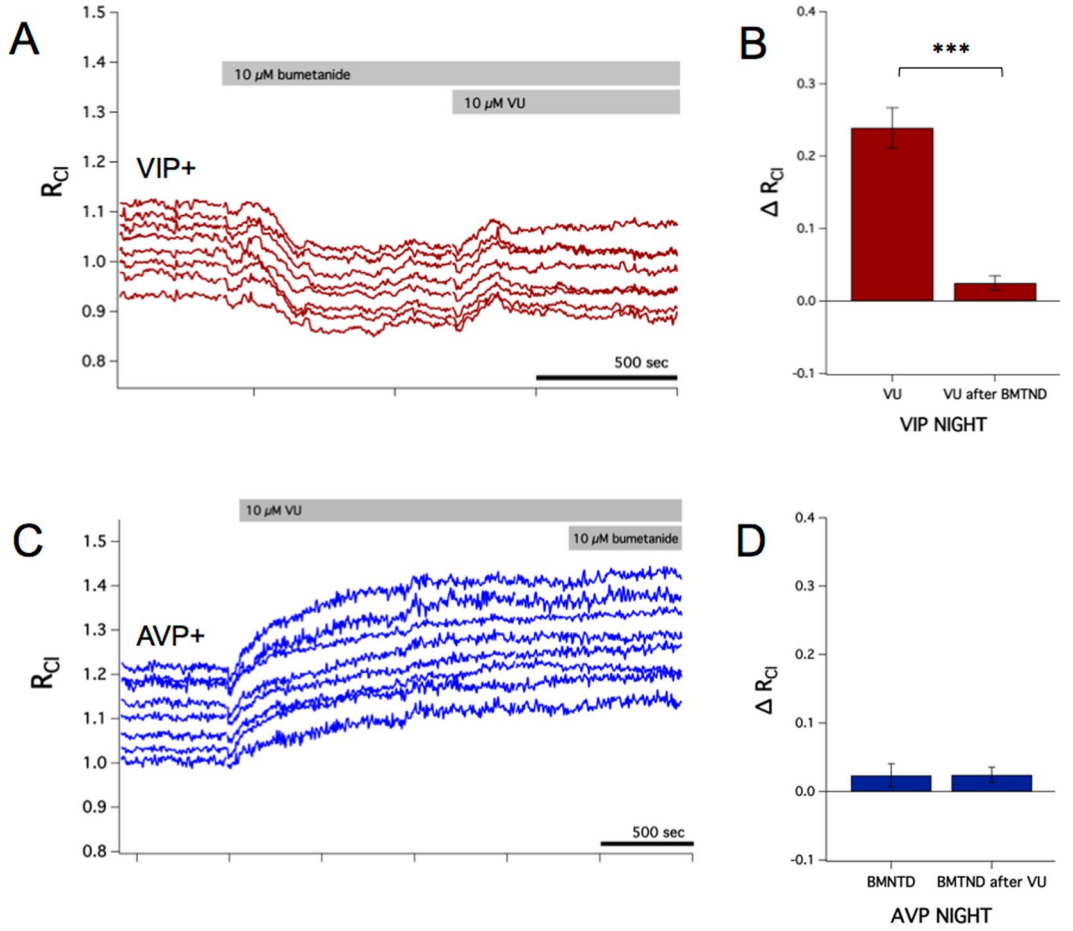

Figure 5. Bumetanide occludes the effect of VU. (**A**) Example experiment from a VIP::Cl-Sensor mouse recorded during the night in which VU (10 μM) was applied after bumetanide (10 μM). From rest, VU elicits a 0.24 increase in R_{Cl} on average (**B**, same data from Fig. 3). However, the effect of VU was occluded in the presence of bumetanide (GEE, $p < 0.001$), suggesting that NKCC1 mediates the Cl^- accumulation elicited by VU. Conversely, the effect of bumetanide in the presence of VU was similar to the effect of bumetanide alone (Fig. C and D), indicating that the KCCs are necessary to mediate Cl^- extrusion in these neurons.

in situ hybridization[65] and immunocytochemical[66] studies have described regional expression of chloride transporters in the rat SCN. Therefore, these regional differences in expression may explain the differential effects of VU and bumetanide in AVP+ and VIP+ neurons. Specifically, KCC2 expression was limited to the ventrolateral SCN, and colocalized with neurons containing GRP or VIP. Markedly, KCC2 expression was absent from the dorsomedial SCN and did not colocalize with AVP—rather, KCC3 and KCC4 were found in the dorsomedial SCN[32]. This histology is in agreement with our observation that VU had a larger effect in VIP+ neurons compared to AVP+ neurons. Despite the paucity of KCC2 in the dorsomedial SCN, we observed that VU increased $[Cl^-]_i$ in AVP+ neurons, albeit less than it did in VIP+ neurons. The efficacy of VU in the AVP+ neurons may be explained by the non-specificity of VU for KCC2[44]. VU may have acted on KCC3 or KCC4 in AVP+ neurons.

Generally, resting membrane potential in SCN neurons is approximately −45 mV during the night and exhibits oscillations of roughly 10 to 15 mV throughout the day[61,67]. For a neuron with a V_m of −45 mV, $[Cl^-]_i$ is passively distributed at approximately 15 mM. Therefore, our estimates of resting $[Cl^-]_i$ (greater than 20 mM) indicate that there are constitutively-active uptake mechanisms in SCN neurons. In VIP+ neurons, blocking NKCC1 decreased $[Cl^-]_i$, supporting a role for NKCC1-mediated Cl^- uptake in setting resting $[Cl^-]_i$. However, in AVP+ neurons, bumetanide caused a small increase in $[Cl^-]_i$, suggesting that other uptake mechanisms are active in AVP+ neurons. Accordingly, Choi *et al*. observed that GABA-induced Ca^{2+} transients remained in NKCC1 knockout mice[15]. This Cl^- uptake may be mediated by the anion exchangers (AEs), which exchange intracellular bicarbonate for extracellular chloride, or could be mediated by a Cl^- channel[12,43]. Indeed, our results in HEPES-buffered solutions, which minimize the presence of bicarbonate transport, imply the presence of bicarbonate-dependent Cl^- regulation in SCN neurons. Although generally similar, the experiments done in HEPES-buffered solution revealed several interesting differences. The effect of bumetanide in AVP+ neurons differed between solutions, and experiments done in HEPES-buffered solution revealed a day/night difference in VU's effect on VIP+ neurons (Figs 3 and 4). These findings implicate the activity of the Na^+-driven Cl-HCO_3

exchanger (NDCBE) or the AE family of cotransporters in SCN neurons. Further research will be necessary to address the role of these transporters in SCN physiology.

Overall, our results demonstrate day/night and regional differences in $[Cl^-]_i$ regulation and highlight the KCC family of chloride co-transporters as regulators of $[Cl^-]_i$ in SCN neurons. Therefore, our results add to a growing number of studies that point to the importance of $[Cl^-]_i$ in SCN function.

Methods

Animal strains and housing. Cl^- imaging experiments were performed with C57BL/6 mice in which a floxed Cl-Sensor allele was inserted into the Rosa26 locus[33]. We crossed these mice with either AVP-IRES-Cre[34] or VIP-IRES-Cre mice[34, 35] to yield AVP::Cl-Sensor or VIP::Cl-Sensor mice. Tail snips were sent to an external facility for genotyping (Transnetyx, Inc). Mice were heterozygous for both the Cl-Sensor and Cre transgenes. Tissue was prepared from adult male and female mice between two and six months old. Electrophysiological experiments were performed on wild type male Wistar rats aged 3 to 9 months.

All animals were entrained to 12:12 light-dark (LD) cycles, with the time of lights on represented as ZT 0. All procedures were approved in advance by the Institutional Animal Care and Use Committee of Oregon Health and Science University, and all experiments were performed in accordance with the approved animal protocol.

Confocal microscopy of fixed tissue. Each mouse was deeply anaesthetized with isoflurane and transcardially perfused with 10 mL of phosphate buffered saline (PBS) followed by 10 mL of 4% paraformaldehyde solution in PBS (pH 7.4). The brain was removed and post-fixed for 1-2 hours at 4 °C in the same solution. After repeated washes in 0.1 M PB, the brain was blocked and secured to a vibratome insert with cyanoacrylate adhesive and agarose supports. Coronal (40 μm thick) sections were cut with a Leica vibratome in 0.1 M PB and subsequently washed in the same buffer. For optical clearing, we treated the tissue with a glycerol/0.1 M PB gradient (25% to 90%). The tissue was incubated in each solution at 4 °C with light agitation until equilibrated. After clearing, sections were transferred into a 10% glycerol/0.1 M PB solution and counterstained with DAPI. Tissue sections were transferred onto glass slides in 10% glycerol solution and the cover glass was mounted with ProLong Diamond media after removing the excess buffer. Images were taken with a Zeiss Axioskop 2 TM fluorescent microscope using AxioVision 4.8 software (Carl Zeiss MicroImaging, Inc.). Confocal micrographs consisted of several 0.4 μm thick optical sections adjusted for optimal brightness and contrast using FIJI software.

Acute slice preparation. During their light phase (ZT 1-3 for day experiments and ZT 10-12 for night experiments), animals were removed from their housing chambers, anaesthetized with isoflurane, and decapitated. The brain was quickly removed and submerged in an ice-cold slicing solution consisting of (in mM): 111 NaCl, 26 $NaHCO_3$, 11 dextrose, 6 Na-gluconate, 4 $MgCl_2$, 3 KCl, 1 NaH_2PO_4, and 0.5 $CaCl_2$, saturated with 95% O_2, 5% CO_2. The brain was blocked and 175 μm thick coronal slices were prepared with a Leica VT1000S vibrating blade microtome. Slices were incubated in slicing solution for 1-4 hours at 34 °C before recording.

Cl^- imaging from acute SCN slices. During image acquisition, slices were perfused at 1–2 mL/min with an artificial cerebrospinal fluid (aCSF) with Cl^- adjusted to the physiological concentration (122 mM; ref. 68). aCSF contained (in mM): 114 NaCl, 26 $NaHCO_3$, 11 dextrose, 6 Na-gluconate, 2.7 KCl, 2 $CaCl_2$, 1 $MgCl_2$, and 1 NaH_2PO_4, saturated with 95% O_2, 5% CO_2. Where indicated, experiments were performed with a HEPES-buffered aCSF containing (in mM): 114 NaCl, 22 Na-gluconate, 12.5 HEPES, 7.5 Na-HEPES, 5 dextrose, 2.7 KCl, 2 $CaCl_2$, 1 $MgCl_2$, and 1 NaH_2PO_4. pH was adjusted to 7.40 with NaOH, and the solution was gassed with 100% O_2. The bath was maintained at 34 °C for all experiments and tetrodotoxin (TTX) was included in recording solutions to eliminate any possible polysynaptic effects of GABA agonists.

Experiments were performed during ZT 2–8 for 'day' mice and ZT 12–18 for 'night' mice. Cl-Sensor fluorescent imaging was performed using epifluorescent methodology similar to that described by Friedel *et al.*[69]. Excitation light was supplied by a monochrometer (Polychrome IV; Till Photonics) providing 10 nm bandwidth output. Excitation at 500 nm preceded excitation at 436 nm to promote Cl-Sensor photostability[69]. Excitation duration ranged from 20 to 200 ms, with the excitation at 500 nm 1.5 times longer than that at 436 nm in order to obtain similar intensity values. The fluorescent signal passed through a double bandpass emission filter [470(24) + 535(30) nm] (Chroma Technology Corporation). Imaging was performed with an upright fluorescent microscope and a 63x water-immersion objective, NA 0.90 (Leica). Images were acquired with a charge-coupled device camera (CCD, ORCA-ER 12 bit level; Hamamatsu). Camera gain was set to 100, and binning was 4×4. Equipment control and image processing were performed with Metafluor software (Molecular Devices). Regions of interest (ROI) were defined around neuronal soma, and a dim region of the field of view was selected as background. Background values were subtracted for each wavelength independently. Because the YFP moiety of Cl-Sensor is quenched by Cl^- ions, we choose to plot the emission following 436 nm excitation over that at 500 nm excitation so that R_{Cl} would be a proxy for $[Cl^-]_i$, with a higher ratio indicating higher $[Cl^-]_i$.

When sampling at 2 and 5 second intervals, an exposure-dependent increase of R_{Cl} was observed, most likely due to an accumulation of Cl-Sensor's YFP moiety in an inactivated state[69]. To correct for this instability, we fit our data with a single-exponential function, and subtracted the time-dependent component. Despite this correction, we observed that steady-state R_{Cl} remained sensitive to exposure duration. We corrected for this exposure-dependent trend in each condition (AVP+ day, AVP+ night, VIP+ day, VIP+ night) independently in order to avoid any assumptions about the similarities of baseline R_{Cl} across conditions. All values were adjusted to a 500 nm exposure of 100 ms.

Calibration of Cl-Sensor and estimation of $[Cl^-]_i$. In order to relate R_{Cl} to $[Cl^-]_i$, it was necessary to construct a calibration curve. Cl-Sensor was calibrated using a 0 mM Cl^- solution consisting of (in mM): 120 Na-gluconate, 26 $NaHCO_3$, 11 dextrose, 2.7 K-gluconate, 2 Ca-gluconate, 1 $MgSO_4$, and 1 NaH_2PO_4, saturated

with 95% O_2, 5% CO_2. This solution was mixed with aCSF to produce solutions of 0, 4, 20, 40, 60, and 80, and 123 mM Cl^-. 50 μM β-escin was added to all calibration solutions to permeabilize cells. AVP::Cl-Sensor and VIP::Cl-Sensor day and night-entrained mice were used for analysis. R_{Cl} values were corrected for exposure as discussed above. Average steady-state R_{Cl} was plotted against Cl^- concentration (Supplementary Fig. 1) and calibration data was fit with the following logistic dose-response sigmoidal curve:

$$R_{Cl} = R_{\max} + \frac{R_{\min} + R_{\max}}{1 + \left(\frac{[Cl^-]_i}{K_d}\right)^p} \quad (1)$$

Where R_{Cl} is the fluorescence intensity ratio (F_{436}/F_{500}) for chloride, K_d is the dissociation constant for Cl^- binding, R_{min} and R_{max} are the minimum and maximum asymptotic values of R_{Cl}, and p is the Hill coefficient[33]. To obtain estimates of $[Cl^-]_i$, we re-arranged the equation for $[Cl^-]_i$:

$$[Cl^-]_i = K_d \times \left(\frac{R_{\min} - R_{\max}}{R_{Cl} - R_{\max}}\right)^{\frac{1}{p}} \quad (2)$$

After fitting the curve, we obtained the following values: $K_d = 108.8$ mM, $R_{min} = 0.98$, $R_{max} = 2.92$ and $p = 2.91$ (Supplementary Fig. 1). Our K_d is considerably higher than previously-reported values[33,70,71]. We also observed substantial variability in R_{Cl} at specific Cl^- concentrations between calibration experiments. Furthermore, R_{Cl} was fairly non-linear in our range of operation (see Supplementary Fig. 1; our R_{Cl} values were generally between 1.0 and 1.3). For these reasons, we elected to leave fluorescent measurements in values of R_{Cl} instead of converting them into estimates of $[Cl^-]_i$ in subsequent analysis.

Perforated-patch electrophysiology. Brain slices were prepared as above. Recordings were performed with an Axopatch-1D amplifier (Axon Instruments), filtered at 2 kHz, digitized at 5 kHz, and acquired with Patchmaster v5.3 (HEKA Elektronik). Pipette solution contained (in mM): 120 KCl, 20 K-gluconate, 15 HEPES, 2 NaCl, 1 EGTA and either 0.2 of Lucifer Yellow or Texas Red. pH was adjusted to 7.26 with KOH. Gramicidin (Sigma) was dissolved in DMSO to a concentration of 50 mg/mL, aliquoted, and frozen. Before an experiment, this stock solution was diluted to a final pipette concentration of 30–100 μg/mL. A drop of gramicidin-free pipette solution was first applied to the backend of the pipette. After capillary action filled the pipette tip, the pipette was back-filled with the gramicidin-containing solution moments before submersion into the recording chamber. After gigaseal formation, series resistance (R_s) was monitored with a −5 mV voltage step to monitor the progress of perforation. Only recordings with a R_s less than 100 MΩ were used for experiments. Cells were voltage clamped at −60 mV and cells with holding currents less than −30 pA were discarded.

E_{GABA} was determined using voltage ramp protocols. Every 10 seconds, a 400 ms voltage ramp protocol ($\Delta V \cong 60$ mV) was executed 100 ms after puff-application of 1 mM GABA. A current trace recorded in the absence of GABA was subtracted from currents obtained in the presence of GABA. The subtracted current trace was then plotted against the ramp command potential, and E_{GABA} was recorded as the x-intercept. E_{GABA} was not corrected for R_s or liquid junction potentials.

Drugs. All drugs used in this study were acquired from Tocris Bioscience. Bumetanide and VU0240551 were dissolved in DMSO, stored as 10 mM stock solutions, and applied through the bath at 10 μM. A 100 mM stock of isoguvacine in water was diluted in aCSF to 1 mM and focally applied (5 psi) through a micropipette connected to a Picospritzer (General Valve Corporation).

Statistics and analysis. Igor Pro (Version 6.22 A; Wavemetrics) was used for plotting, curve-fitting and data analysis. Data are presented as the mean ± standard error. For imaging experiments, generalized estimating equations (GEE) were used to determine statistical significance[72]. GEE models are similar to ANOVA and general linear models in that they estimate a mean response, except standard errors are adjusted for clustered or correlated measurements that originate from multiple observations made from the same brain slice. Therefore, each brain slice is treated as an independent measure, while the ROIs influence the average and standard error of each experiment. GEE test statistics are based on chi-square or z-statistics rather than F- and t-distributions. When comparing drug effects between HEPES-buffered and bicarbonate-buffered solutions, we formed z-statistics equal to the difference between the estimated effects from each separate GEE model (one for each solution) divided by the standard error of the difference. Significance level was Bonferroni-adjusted for these comparisons. For electrophysiology experiments, we used the Student's *t*-test. For all tests, a *p*-value less than 0.05 was considered to be statistically significant.

Data availability. The datasets generated during and/or analyzed during the current study are available from the corresponding author on reasonable request.

References

1. Moldavan, M. G., Irwin, R. P. & Allen, C. N. Presynaptic $GABA_B$ receptors Regulate Retinohypothalamic Tract Synaptic Transmission by inhibiting Voltage-Gated Ca^{2+} Channels. *Journal of neurophysiology* **95**, 3727–3741 (2006).
2. Gillespie, C. F., Huhman, K. L., Babagbemi, T. O. & Albers, H. E. Bicuculline increases and muscimol reduces the phase-delaying effects of light and VIP/PHI/GRP in the suprachiasmatic region. *Journal of biological rhythms* **11**, 137–144 (1996).
3. Gillespie, C. F., Mintz, E. M., Marvel, C. L., Huhman, K. L. & Albers, H. E. GABAA and GABAB agonists and antagonists alter the phase-shifting effects of light when microinjected into the suprachiasmatic region. *Brain Res* **759**, 181–189 (1997).

4. Kononenko, N. I. & Dudek, F. E. Mechanism of irregular firing of suprachiasmatic nucleus neurons in rat hypothalamic slices. *Journal of neurophysiology* **91**, 267–273 (2004).
5. Liu, C. & Reppert, S. M. GABA synchronizes clock cells within the suprachiasmatic circadian clock. *Neuron* **25**, 123–128 (2000).
6. Albus, H., Vansteensel, M. J., Michel, S., Block, G. D. & Meijer, J. H. A GABAergic mechanism is necessary for coupling dissociable ventral and dorsal regional oscillators within the circadian clock. *Curr Biol* **15**, 886–893 (2005).
7. Freeman, G. M. Jr., Krock, R. M., Aton, S. J., Thaben, P. & Herzog, E. D. GABA Networks Destabilize Genetic Oscillations in the Circadian Pacemaker. *Neuron* **78**, 799–806 (2013).
8. Evans, J. A., Leise, T. L., Castanon-Cervantes, O. & Davidson, A. J. Dynamic interactions mediated by nonredundant signaling mechanisms couple circadian clock neurons. *Neuron* **80**, 973–983 (2013).
9. DeWoskin, D. *et al*. Distinct roles for GABA across multiple timescales in mammalian circadian timekeeping. *Proceedings of the National Academy of Sciences of the United States of America* **112**, E3911–3919 (2015).
10. Gamba, G. Molecular physiology and pathophysiology of electroneutral cation-chloride cotransporters. *Physiological reviews* **85**, 423–493 (2005).
11. Ben-Ari, Y. *et al*. Refuting the challenges of the developmental shift of polarity of GABA actions: GABA more exciting than ever! *Frontiers in cellular neuroscience* **6**, 35 (2012).
12. Blaesse, P., Airaksinen, M. S., Rivera, C. & Kaila, K. Cation-chloride cotransporters and neuronal function. *Neuron* **61**, 820–838 (2009).
13. Wagner, S., Castel, M., Gainer, H. & Yarom, Y. GABA in the mammalian suprachiasmatic nucleus and its role in diurnal rhythmicity. *Nature* **387**, 598–603 (1997).
14. De Jeu, M. & Pennartz, C. M. A. Circadian modulation of GABA function in the rat suprachiasmatic nucleus: excitatory effects during the night phase. *Journal of neurophysiology* **87**, 834–844 (2002).
15. Choi, H. J. *et al*. Excitatory Actions of GABA in the Suprachiasmatic Nucleus. *J Neurosci* **28**, 5450–5459 (2008).
16. Irwin, R. P. & Allen, C. N. GABAergic signaling induces divergent neuronal Ca(2+) responses in the suprachiasmatic nucleus network. *The European journal of neuroscience* **30**, 1462–1475 (2009).
17. Alamilla, J., Perez-Burgos, A., Quinto, D. & Aguilar-Roblero, R. Circadian modulation of the cl(−) equilibrium potential in the rat suprachiasmatic nuclei. *BioMed research international* **2014**, 424982 (2014).
18. Farajnia, S., van Westering, T. L., Meijer, J. H. & Michel, S. Seasonal induction of GABAergic excitation in the central mammalian clock. *Proceedings of the National Academy of Sciences of the United States of America* **111**, 9627–9632 (2014).
19. Fan, J. *et al*. Vasoactive intestinal polypeptide (VIP)-expressing neurons in the suprachiasmatic nucleus provide sparse GABAergic outputs to local neurons with circadian regulation occurring distal to the opening of postsynaptic GABAA ionotropic receptors. *J Neurosci* **35**, 1905–1920 (2015).
20. Wagner, S., Sagiv, N. & Yarom, Y. GABA-induced current and circadian regulation of chloride in neurones of the rat suprachiasmatic nucleus. *The Journal of physiology* **537**, 853–869 (2001).
21. Itri, J., Michel, S., Waschek, J. A. & Colwell, C. S. Circadian rhythm in inhibitory synaptic transmission in the mouse suprachiasmatic nucleus. *Journal of neurophysiology* **92**, 311–319 (2004).
22. Gompf, H. S. & Allen, C. N. GABAergic synapses of the suprachiasmatic nucleus exhibit a diurnal rhythm of short-term synaptic plasticity. *European Journal of Neuroscience* **19**, 2791–2798 (2004).
23. Myung, J. *et al*. GABA-mediated repulsive coupling between circadian clock neurons in the SCN encodes seasonal time. *Proceedings of the National Academy of Sciences of the United States of America* **112**, E3920–3929 (2015).
24. Bormann, J., Hamill, O. P. & Sakmann, B. Mechanism of anion permeation through channels gated by glycine and G-aminobutyric acid in mouse cultured spinal cord neurones. *The Journal of physiology (london)* **385**, 243–286 (1987).
25. Kaila, K. & Voipio, J. Postsynaptic fall in intracellular pH induced by GABA-activated bicarbonate conductance. *Nature* **330**, 163–165 (1987).
26. Farrant, M. & Kaila, K. The cellular, molecular and ionic basis of GABA(A) receptor signalling. *Progress in brain research* **160**, 59–87 (2007).
27. Lu, J., Karadsheh, M. & Delpire, E. Developmental regulation of the neuronal-specific isoform of K-Cl cotransporter KCC2 in postnatal rat brains. *Journal of neurobiology* **39**, 558–568 (1999).
28. Williams, J. R., Sharp, J. W., Kumari, V. G., Wilson, M. & Payne, J. A. The neuron-specific K-Cl cotransporter, KCC2. Antibody development and initial characterization of the protein. *The Journal of biological chemistry* **274**, 12656–12664 (1999).
29. Mercado, A., Broumand, V., Zandi-Nejad, K., Enck, A. H. & Mount, D. B. A C-terminal domain in KCC2 confers constitutive K+ -Cl- cotransport. *The Journal of biological chemistry* **281**, 1016–1026 (2006).
30. Strange, K., Singer, T. D., Morrison, R. & Delpire, E. Dependence of KCC2 K-Cl cotransporter activity on a conserved carboxy terminus tyrosine residue. *Am J Physiol Cell Physiol* **279**, C860–867 (2000).
31. Song, L. *et al*. Molecular, functional, and genomic characterization of human KCC2, the neuronal K-Cl cotransporter. *Brain Res Mol Brain Res* **103**, 91–105 (2002).
32. Belenky, M. A. *et al*. Cell-type specific distribution of chloride transporters in the rat suprachiasmatic nucleus. *Neuroscience* **165**, 1519–1537 (2010).
33. Batti, L. *et al*. Transgenic mouse lines for non-invasive ratiometric monitoring of intracellular chloride. *Front Mol Neurosci* **6**, 11 (2013).
34. Harris, J. A. *et al*. Anatomical characterization of Cre driver mice for neural circuit mapping and manipulation. *Frontiers in neural circuits* **8**, 76 (2014).
35. Taniguchi, H. *et al*. A resource of cre driver lines for genetic targeting of GABAergic neurons in cerebral cortex. *Neuron* **71**, 995–1013 (2011).
36. Van den Pol, A. N. Gamma-aminobutyrate, gastrin releasing peptide, serotonin, somatostatin, and vasopressin: ultrastructural immunocytochemical localization in presynaptic axons in the suprachiasmatic nucleus. *Neuroscience* **17**, 643–659 (1986).
37. Haam, J. *et al*. GABA Is Excitatory in Adult Vasopressinergic Neuroendocrine Cells. *J Neurosci* **32**, 572–582 (2012).
38. Arosio, D. & Ratto, G. M. Twenty years of fluorescence imaging of intracellular chloride. *Frontiers in cellular neuroscience* **8**, 258 (2014).
39. Mukhtarov, M. *et al*. Calibration and functional analysis of three genetically encoded Cl(-)/pH sensors. *Front Mol Neurosci* **6**, 9 (2013).
40. Raimondo, J. V. *et al*. A genetically-encoded chloride and pH sensor for dissociating ion dynamics in the nervous system. *Frontiers in cellular neuroscience* **7**, 202 (2013).
41. Staley, K. J. & Proctor, W. R. Modulation of mammalian dendritic GABA(A) receptor function by the kinetics of Cl- and HCO3- transport. *The Journal of physiology* **519**, 693–712 (1999).
42. Lamsa, K. & Taira, T. Use-dependent shift from inhibitory to excitatory GABAA receptor action in SP-O interneurons in the rat hippocampal CA3 area. *Journal of neurophysiology* **90**, 1983–1995 (2003).
43. Doyon, N., Vinay, L., Prescott, S. A. & De Koninck, Y. Chloride Regulation: A Dynamic Equilibrium Crucial for Synaptic Inhibition. *Neuron* **89**, 1157–1172 (2016).
44. Delpire, E. *et al*. Small-molecule screen identifies inhibitors of the neuronal K-Cl cotransporter KCC2. *Proceedings of the National Academy of Sciences of the United States of America* **106**, 5383–5388 (2009).
45. Russell, J. M. Sodium-potassium-chloride cotransport. *Physiological reviews* **80**, 211–276 (2000).
46. Liou, S. Y. & Albers, H. E. Single unit response of neurons within the hamster suprachiasmatic nucleus to GABA and low chloride perfusate during the day and night. *Brain research bulletin* **25**, 93–98 (1990).
47. Mason, R., Biello, S. M. & Harrington, M. E. The effects of GABA and benzodiazepines on neurones in the suprachiasmatic nucleus (SCN) of Syrian hamsters. *Brain Res* **552**, 53–57 (1991).

48. Bos, N. P. A. & Mirmiran, M. Effects of excitatory and inhibitory amino acids on neuronal discharges in the cultured suprachiasmatic nucleus. *Brain research bulletin* **31**, 67–72 (1993).
49. Chen, G., Trombley, P. & Van den Pol, A. N. Excitatory actions of GABA in developing rat hypothalamic neurones. *The Journal of physiology (london)* **494**, 451–464 (1996).
50. Welsh, D. K., Takahashi, J. S. & Kay, S. A. Suprachiasmatic nucleus: cell autonomy and network properties. *Annual review of physiology* **72**, 551–577 (2010).
51. Lee, I. T. *et al*. Neuromedin s-producing neurons act as essential pacemakers in the suprachiasmatic nucleus to couple clock neurons and dictate circadian rhythms. *Neuron* **85**, 1086–1102 (2015).
52. Tremere, L. A., Pinaud, R., Irwin, R. P. & Allen, C. N. Postinhibitory rebound spikes are modulated by the history of membrane hyperpolarization in the SCN. *The European journal of neuroscience* **28**, 1127–1135 (2008).
53. Delpire, E. & Staley, K. J. Novel determinants of the neuronal Cl- concentration. *The Journal of physiology*, (2014).
54. Chamma, I., Chevy, Q., Poncer, J. C. & Levi, S. Role of the neuronal K-Cl co-transporter KCC2 in inhibitory and excitatory neurotransmission. *Frontiers in cellular neuroscience* **6**, 5 (2012).
55. Dzhala, V., Valeeva, G., Glykys, J., Khazipov, R. & Staley, K. Traumatic alterations in GABA signaling disrupt hippocampal network activity in the developing brain. *J Neurosci* **32**, 4017–4031 (2012).
56. Kahle, K. T. *et al*. Roles of the cation-chloride cotransporters in neurological disease. *Nat Clin Pract Neurol* **4**, 490–503 (2008).
57. Campos, L. M., Cruz-Rizzolo, R. J., Watanabe, I. S., Pinato, L. & Nogueira, M. I. Efferent projections of the suprachiasmatic nucleus based on the distribution of vasoactive intestinal peptide (VIP) and arginine vasopressin (AVP) immunoreactive fibers in the hypothalamus of Sapajus apella. *Journal of chemical neuroanatomy* **57-58**, 42–53 (2014).
58. Gribkoff, V. K. *et al*. A reexamination of the role of GABA in the mammalian suprachiasmatic nucleus. *Journal of biological rhythms* **14**, 126–130 (1999).
59. Khawaled, R., Bruening-Wright, A., Adelman, J. P. & Maylie, J. Bicuculline block of small-conductance calcium-activated potassium channels. *Pflugers Archiv. European Journal of Physiology* **438**, 314–321 (1999).
60. Teshima, K., Kim, S. H. & Allen, C. N. Characterization of an apamin-sensitive potassium current in suprachiasmatic nucleus neurons. *Neuroscience* **120**, 65–73 (2003).
61. Belle, M. D., Diekman, C. O., Forger, D. B. & Piggins, H. D. Daily electrical silencing in the mammalian circadian clock. *Science* **326**, 281–284 (2009).
62. Wright, R., Raimondo, J. V. & Akerman, C. J. Spatial and temporal dynamics in the ionic driving force for GABA(A) receptors. *Neural Plast* **2011**, 728395 (2011).
63. Duebel, J. *et al*. Two-photon imaging reveals somatodendritic chloride gradient in retinal ON-type bipolar cells expressing the biosensor Clomeleon. *Neuron* **49**, 81–94 (2006).
64. Glykys, J. *et al*. Local impermeant anions establish the neuronal chloride concentration. *Science* **343**, 670–675 (2014).
65. Kanaka, C. *et al*. The differential expression patterns of messenger RNAs encoding K-Cl cotransporters (KCC1,2) and Na-K-2Cl cotransporter (NKCC1) in the rat nervous system. *Neuroscience* **104**, 933–946 (2001).
66. Belenky, M. A., Yarom, Y. & Pickard, G. E. Heterogeneous expression of gamma-aminobutyric acid and gamma-aminobutyric acid-associated receptors and transporters in the rat suprachiasmatic nucleus. *The Journal of comparative neurology* **506**, 708–732 (2008).
67. Kuhlman, S. J. & McMahon, D. G. Rhythmic regulation of membrane potential and potassium current persists in SCN neurons in the absence of environmental input. *The European journal of neuroscience* **20**, 1113–1117 (2004).
68. Schrock, H. & Kuschinsky, W. Cerebrospinal fluid ionic regulation, cerebral blood flow, and glucose use during chronic metabolic alkalosis. *The American journal of physiology* **257**, H1220–1227 (1989).
69. Friedel, P., Bregestovski, P. & Medina, I. Improved method for efficient imaging of intracellular Cl(−) with Cl-Sensor using conventional fluorescence setup. *Front Mol Neurosci* **6**, 7 (2013).
70. Markova, O., Mukhtarov, M., Real, E., Jacob, Y. & Bregestovski, P. Genetically encoded chloride indicator with improved sensitivity. *Journal of neuroscience methods* **170**, 67–76 (2008).
71. Waseem, T., Mukhtarov, M., Buldakova, S., Medina, I. & Bregestovski, P. Genetically encoded Cl-Sensor as a tool for monitoring of Cl-dependent processes in small neuronal compartments. *Journal of neuroscience methods* (2010).
72. Zeger, S. L. & Liang, K. Y. Longitudinal data analysis for discrete and continuous outcomes. *Biometrics* **42**, 121–130 (1986).

Acknowledgements

We thank Dr. Piotr Bregestovski for kindly providing us with the Cre-inducible Rosa26::Cl-Sensor mice and Mike Lasarev for help with statistical analysis. Olga Cravetchi managed the mouse breeding and genotyping. The work was supported by National Institutes of Health (NIH) grant NS036607 and a Medical Research Foundation of Oregon grant to CNA.

Author Contributions

N.J.K. and C.N.A. designed the experiments. N.J.K. performed the experiments and analyzed the data. N.J.K. and C.N.A. wrote and edited the manuscript.

Additional Information

Supplementary information accompanies this paper at doi:10.1038/s41598-017-09778-x

Competing Interests: The authors declare that they have no competing interests.

Publisher's note: Springer Nature remains neutral with regard to jurisdictional claims in published maps and institutional affiliations.